Journal of the Serbian Chemical Society
JSCS-info@shd.org.rs • www.shd.org.rs/JSCS
J. Serb. Chem. Soc. *86* (3) 327–340 (2021)
JSCS–5424
Original scientific paper

Role of EDTA capped cobalt oxide nanomaterial in photocatalytic degradation of dyes

MEENA SINGH[1], DIPTI VAYA[2]*, RAVI KUMAR[3] and BIJOY K. DAS[1]

[1]*Department of Applied Science, The NorthCap University, Sector 23A, Gurugram-122017, India,* [2]*Department of Chemistry, Amity School of Applied Sciences, Amity University Haryana, Gurugram-122413, India and* [3]*Department of Chemistry, NIT, Srinagar, Jammu and Kasmir-190006, India*

(Received 11 July, revised 4 October, accepted 16 November 2020)

Abstract: Dyes released from textile, paint, and various other industries in wastewater have posed long term environmental damage. Functional nanomaterials provide a hope and opportunities to treat these effluent wastes in a rapid and efficient way due to their large surface area to volume ratios. Synthesis of 2,2',2",2"'-(ethane-1,2-diyldinitrilo)tetraacetic acid (EDTA) capped cobalt oxide nanomaterial, as a photocatalyst, has been investigated and used for the rapid and efficient removal of malachite green (MG) and crystal violet (CV) dyes. The morphological, structural, optical, chemical and thermal properties of the synthesized nanomaterial were analysed using different characterization tools such as scanning electron microscopy, transmission electron microscopy, X-ray diffraction, ultra violet–visible and Fourier transform infrared (FT-IR) spectroscopy and thermogravimetric analysis. The prepared EDTA capped cobalt oxide nanomaterials display better photocatalytic degradation, 56.3 % for MG and 37.9 % for CV in comparison to the pure cobalt oxide, 47.7 and 27.6 %, respectively, under visible light illumination. The kinetics of the degradation followed the pseudo-first order and it corresponds to Freundlich adsorption isotherm model. The incremental photodegradation of these two dyes was attributed by morphology of the nanomaterial which favour effective electron/hole separation.

Keywords: photocatalytic activity; crystal violet; malachite green; adsorption isotherm.

INTRODUCTION

Dye stuffs represent a class of synthetic organic pigments; these are one of the many causes for growing ecological issues. Coloured dyeing wastewaters emanating from industries are largely non-biodegradable and also carcinogenic in nature. They also problems with creating the aquatic creatures and adversely

* Corresponding author. E-mail: diptivaya08@gmail.com
https://doi.org/10.2298/JSC200711074S

affect water ecosystem.[1] Therefore, degradation of dyes has attracted attention and substantial efforts have been committed to the specific remediation techniques. These techniques could degrade bio-recalcitrant organic contaminants into non-toxic form before their discharge into water to decrease the pollution load on mainstream water.

A number of methods such as biodegradation, ozonation, chemical degradation, oxidation, reduction, precipitation, flocculation, photolysis, adsorption, and advanced oxidation process, *etc.*[2,3] have been used to investigate the removal of the dyeing from wastewater. However, heterogeneous photocatalysis, using semiconductor oxides under UV/Vis light, expresses immense potential to convert these organic pollutants into reasonably harmless end products such as CO_2, H_2O and inorganic ions with the possibility of regeneration.[4] Photocatalysis offers good advantage over other conventional methods, as it uses a renewable and ecologically favourable source of energy like sunlight and has many other benefits such as easily controlled simple instrumentation and non-selective oxidation. Semiconducting materials, including TiO_2,WO_3, Ta_2O_5, TiO_2, ZnO, ZrO_2, CdS, MoS_2, Fe_2O_3, ZnS and CdS have been used as heterogeneous photocatalysts for the efficient photodegradation of several organic pollutants present in waste water.[5]

The applicability of heterogeneous catalysts can be improved by modulating their particle size, morphology, size distribution and dispersion. Nanomaterials possessing attractive physical and chemical properties, such as higher surface area to volume ratio and new interfacial properties, that could be used to enhance the photocatalytic process.[6] The semiconductor metal oxide nanoparticles show size dependent optical properties.[7,8]

Magnetic spinel p-type semiconductor Co_3O_4 is a technologically important oxide. A number of different methods for the synthesis of cobalt oxide nanoparticles such as coprecipitation, sol–gel, thermal decomposition, pulsed laser deposition and solution combustion[9–13] were reported. The sol–gel method has acquired more curiosity among researchers in the synthesis of nanoparticles as it offers controlled consolidation, shape modulation and patterning of the nanostructures.[14,15] However, literature survey shows that very small nanoparticles have an extremely high surface area to volume ratio hence, they agglomerate easily to minimize their surface, but size can be controlled by tuning their surface, which can be achieved by capping.[8,16] The nature and the critical concentration of the capping agents controls the morphology of the synthesized nanoparticles.[17]

MG and CV are typical basic triarylmethane cationic dyes. They are used extensively as colouring agents in industries.[18,19] The cationic dyes are more poisonous as they can easily enter the cells through the negatively charged cells membrane surfaces and accumulate in the cytoplasm.[20,21] Both dyes are carcinogenic and pose environmental risks, as MG dye and its reduced form has adverse

effects on the reproductive and the immune system[22] and CV is a mutagen and mitotic poison.[23] The excess inhalation of these dyes cause irritation of the respiratory tracts, vomiting, diarrhoea, headache, dizziness and its long term exposure might damage the mucous membrane and the gastrointestinal tract.[24]

The activity of cobalt oxide nanoparticles is influenced by several factors such as crystallinity, particle size, surface area and method of preparation. The studies reflect Co_3O_4 used in applications such ceramics, pigments, electrochemical devices, solid state sensors, lithium ion batteries, gas sensors, magnetic storage and supercapacitors.[25–27] However, its photocatalytic property has been occasionally observed.[28,29]

The target of the present study is to synthesize photocatalytic active EDTA supported stable cobalt oxide nanomaterial by green chemistry approach and its application in the effectively degradation of MG and CV dyes in aqueous solution. The possible mechanism for photocatalytic degradation of the dyes based on experimental results has also been proposed.

EXPERIMENTAL

All chemicals are analytical grade purchased from Merck and Fischer Scientific. Deionised water was used in all experiments.

Synthesis of EDTA capped cobalt oxide nanomaterial

EDTA supported cobalt oxide nanomaterials were synthesized using the sol–gel method. In brief, aqueous $Co(NO_3)_2{\cdot}H_2O$ of 0.2 M was taken as precursor and 1.0 M NaOH solution was added to it slowly in drops under continuous stirring until basic medium (pH 9) was achieved. Stoichiometric ratio of aqueous solution of capping agent EDTA was prepared and then mixed dropwise with the above basic solution. Thereafter, the reaction mixture was refluxed at 70–80 °C for 15 h until a gel-like compound was formed. The gel was ripened for 12 h and afterwards heated at 200 °C in air oven for 2–3 h to get EDTA supported cobalt oxide nanomaterial (ECO). Finally, ECO was ground in mortar and pestle and stored in desiccators. Similar method is used for the synthesis of cobalt oxide nanomaterials without using EDTA (CO).

Characterization of nanomaterials

The structural and phase crystallinity of the ECO was done using PXRD on Bruker AXS D8 Advance with Cu X-ray wavelength 1.5406 Å at a 2θ scan rate of 0.5°/min, the surface morphology and particles size was investigated using SEM (Zeiss EVO 18) and TEM (Jeol JEM 2100). Functionalities and thermal properties of the capping molecule were investigated using FT-IR spectroscopy and TGA (STA 8000 Perkin Elmer). FT-IR spectra were recorded in the wave number range of 4000 to 400 cm^{-1} using KBr pellets. UV–Vis-NIR spectrophotometer (Cary 5000 Series) was used to record the absorbance spectra of the solid sample. Light intensity was measured by solarimeter.

Photocatalytic activity

MG (C.I. 93405) and CV (C.I. 42555) are organic dyes with chemical formulas $C_{23}H_{25}N_2Cl$ and $C_{25}H_{30}N_3Cl$. Prior to start the photocatalytic activity, the optimization parameters of reaction have been measured, these are: pH 7.5, dye concentration = 10^{-5} M, catalyst amount = 20 mg, light intensity = 60 W cm^{-2}. Then aqueous solutions of optimum concentrat-

ion of dyes (10^{-5} M) and catalyst ECO was taken in beakers. These are placed in dark to attain adsorption and absorption equilibrium and then put under the simulated sunlight of 60 W cm^{-2}. A water filter was used to cut off thermal radiations from the light. Aliquot samples of 5 mL were pipette out at regular interval of 10 min and their absorbance value was monitored at a wavelength of λ_{max} = 610 nm for MG and 590 nm for CV. These values track the photocatalytic progress of these two dyes. Control photocatalysis test with pure cobalt oxide catalyst (CO) was also performed concurrently under similar conditions for comparison. The degradation efficiency of dyes over CO and ECO samples were estimated by:

$$\text{Degradation, \%} = 100\frac{A_0 - A_t}{A_0} \quad (1)$$

where, A is initial absorbance and A_t is absorbance of the dye at t time. Photocatalysis experiments were performed at room temperature. Blank experiments were carried out by irradiating the aqueous solutions of the dyes in the absence of catalyst sample.

RESULT AND DISCUSSION

PXRD of the synthesized nanomaterial measured at 2θ of 20–80° (Fig. 1). These diffraction peaks best matched with Co_3O_4 nanomaterial with JCPDS card No. 09-418. Sample of ECO exhibits few more peak due to capping material, *i.e.*, sodium tetraacetate. From Fig. 1a and b, series of well defined peaks are: 20.06 (111), 31.4 (220), 37.04 (311), 45.06 (400), 59.3 (511) and 65.38° (440), measured which show FCC phase of Co_3O_4 material with Fd3m space group. Sharpness of majority of peaks indicated good degree of crystallinity. In addition, broadening of few peaks was explained by nanometer size range of Co_3O_4. The crystallite size, D, of the nanoparticles was estimated by the Debye–Scherrer formula:

$$D = K\lambda/\beta\cos\theta \quad (2)$$

where, K = Scherrer constant (*i.e.*, 0.94), λ = 0.15406 nm, β = full width at half-maximum (FWMH) of the (311) PXRD peak and θ = Bragg diffraction angle. The computed crystallite sizes were found to be 70 and 43 nm for CO and ECO nanomaterials.

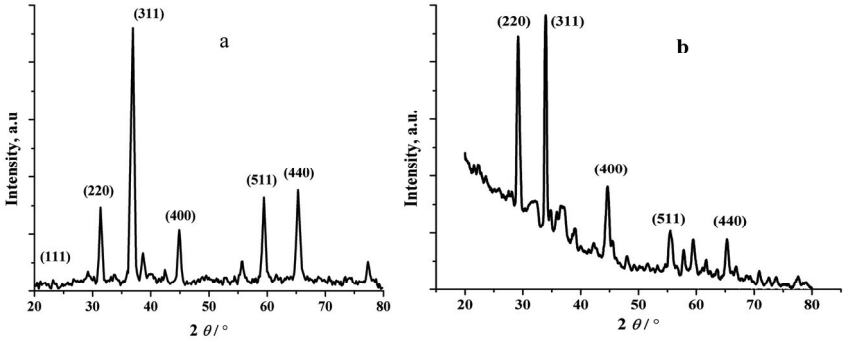

Fig. 1. PXRD of: a) CO and b) ECO.

SEM photograph of CO and ECO revealed the surface texture, porosity and structure of the synthesized nanomaterial. EDTA is an outstanding metal ion chelating agent with six coordinating sites, *i.e.*, two nitrogen and four hydroxyl groups. Hence, surface functionalization through coordination bonds ceased the nucleation growth of the particles and also effectively stabilized them against further oxidation. Nanomaterials exhibited polyhedral shapes with dimensions range from 200 to 300 nm (Fig. 2b). Their porous morphology exposed greater surface area and more reactive sites. CO powder (Fig. 2a) had no particular morphology and the particles are present as highly agglomerated structures.

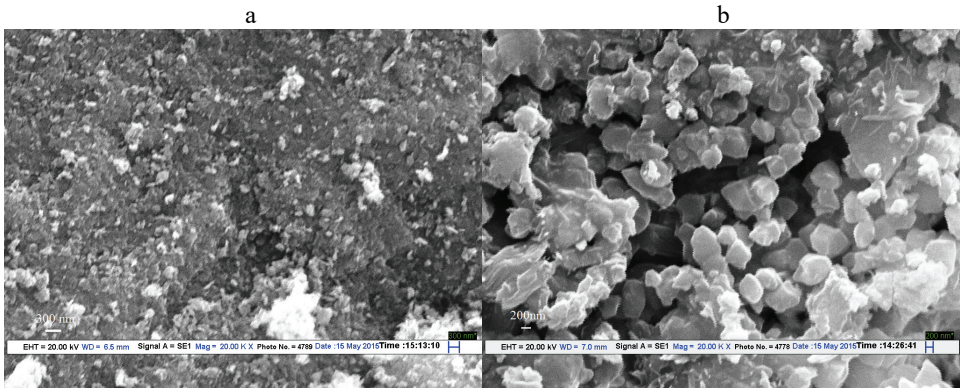

Fig. 2. SEM micrographs of: a) CO and b) ECO.

TEM images of Fig. 3a–d of ECO revealed that the cobalt oxide is capped. Fig. 3c, indicates that the average nanosize of embedded cobalt oxide is 40 nm with nearly spherical morphology matches with XRD crystalline size. SAED pattern of ECO nanomaterial was shown in Fig. 3d where the appearance of diffraction rings and bright spots represent the good degree of crystallinity. This data matches very well with the reported XRD patterns.

The absorption curve (Fig. 4) of ECO and CO for the samples represent two strong absorption bands in 250–350 nm and 400–580 nm wavelength ranges. The first band may be assigned to the charge transfer process from O^{2-} to Co^{2+} while the second one represents O^{2-} to Co^{3+}.[30] It is explicable from the optical absorption spectra that the absorption onset is almost the same for the uncapped and capped samples, as well as the absorption peaks, are without any significant blue shift, probably due to uneven distribution of the synthesized particles. ECO showed lower absorption than CO, suggested the morphological changes of the nanoparticles. This suggested slight variation in band gap which is confirmed by Tauc plot. The value of band gap is determined to be 1.80 and 2.80 eV for ECO and CO, respectively, by plotting graph between energy verses $(\alpha hc/\lambda)^2$. It has also been suggested that the absorption also depends on particle size as reported.[15]

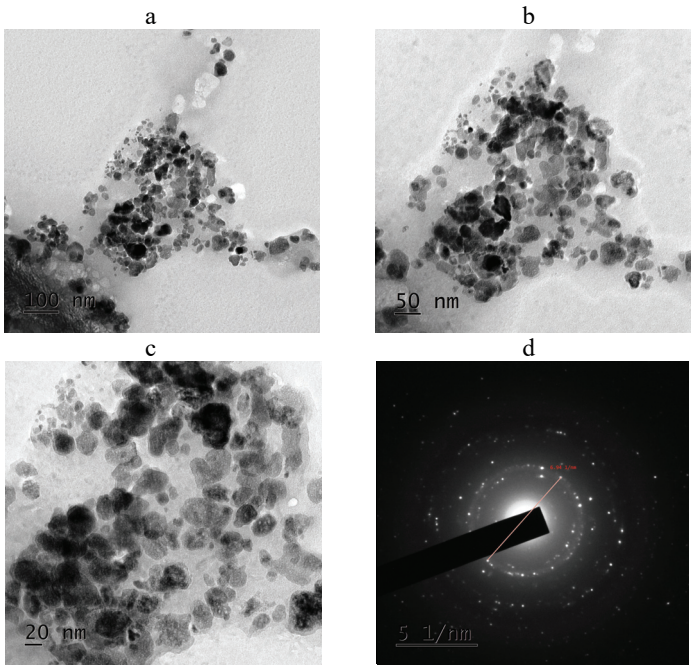

Fig. 3. a–c) Images of TEM at different scales; d) SAED image of TEM.

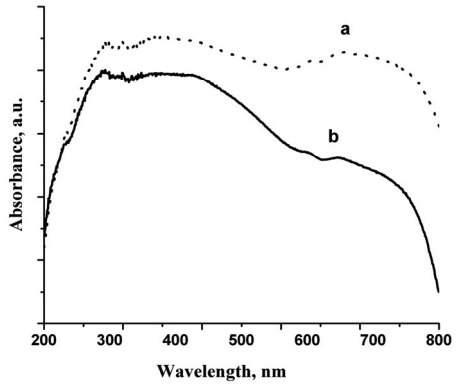

Fig. 4. Optical absorption spectra of: a) CO and b) ECO.

In distinction with the FT-IR spectra of pure EDTA, ECO spectrum is highly resolved (Fig. 5a and b). The spectrum of ECO as represented is broad and few peaks with low transmittance, confirming the complexation of EDTA. The sharp strong absorption band at 1700 cm^{-1} of –C=O stretch of COOH shifted to 1630 cm^{-1} as compare to pure EDTA.[31] This shifting confirmed that EDTA has been encapsulated the Co_3O_4 nanocrystals through esterification between carboxylate group present in EDTA and hydroxyl groups on the Co_3O_4 nanomaterial surface[32–35] and develop a partial single bond character to the –C=O. The broad

absorption band in the higher frequency region of ECO spectrum around 3457 cm^{-1} was associated with hydrogen bond –OH stretching vibration mode of EDTA. The –CN stretch at 1192 cm^{-1} in pure EDTA,[31] shifted to 1177 cm^{-1} in ECO. The sharp and strong absorption band at 1383 cm^{-1} would be the bending vibrations of –CH of methylene groups of EDTA. The sharp peak was at 847 cm^{-1} due to –CH and –OH out of plane bending vibrations. The sharp band around 588 cm^{-1} and shoulder at 662 cm^{-1} characteristics of Co–O stretching and O–Co–O bridging vibrations, respectively, are present in the spectrum of CO even stronger than ECO.

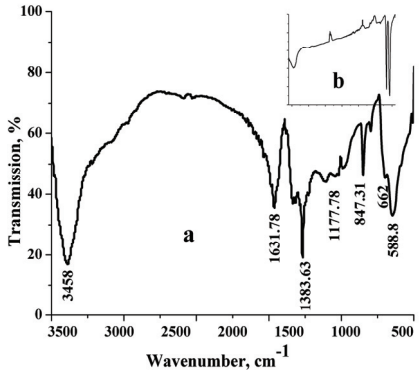

Fig. 5. FTIR spectra of: a) CO and b) ECO.

TGA analysis of ECO performed from room temperature to 700 °C. ECO sample represent 2 steps of thermal degradation. ECO sample exhibited 15 % loss due to moisture removal till 200 °C. After 200 °C sudden reduction of mass is occurred between 210–350 °C, which is attributed to the decomposition of ligand, *i.e.*, EDTA and removal of nitrous oxide, acid moieties as shown in Fig. 6. Above 600 °C again mass reduced due to the formation of CoO from Co_3O_4.

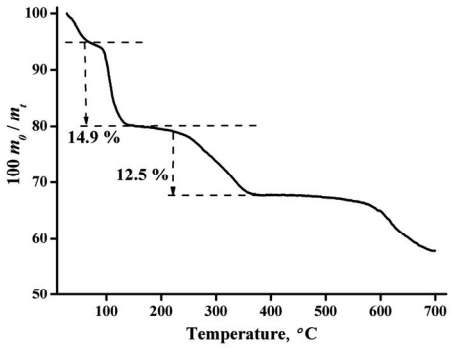

Fig. 6. TGA graph of ECO.

A number of isotherm models such as Langmuir, Freundlich, *etc.* have already been reported to explain the relationship between the amount of ads-

orbate per unit mass of adsorbent. Here, Langmuir and Freundlich isotherm models were used for the isotherm studies by varying the concentration of MG solution from 10 to 150 mg L^{-1}. The well-known linearized equation of Langmuir isotherm model is represented as:

$$\frac{C_e}{Q_e} = \frac{1}{Q_o K_L} + \frac{1}{Q_o} C_e \tag{3}$$

where C_e is the equilibrium concentration in mg L^{-1}, Q_e is the amount of adsorbate adsorbed at equilibrium in mg g^{-1} and Q_o / mg g^{-1} and K_L / L mg^{-1} are the Langmuir constants related to the adsorption capacity and the rate of adsorption, respectively. When C_e/Q_e *vs.* C_e was plotted, a straight line with slope $1/Q_o$ and intercept $1/(Q_o K_L)$ is obtained as shown in Fig. 7a. From these, Langmuir constants Q_o and K_L were calculated and are listed in Table I. The lower value of correlation coefficients R^2 displays that the adsorption does not follows Langmuir isotherm model.

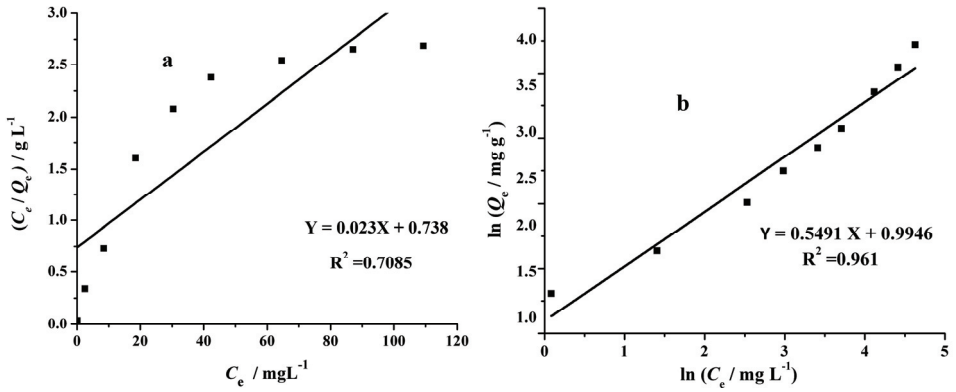

Fig. 7. Adsorption isotherms; a) Langmuir b) Freundlich.

The Freundlich isotherm model reflects as multilayer adsorption. The linearized form of Freundlich isotherm:

$$\ln Q_e = \ln K_F + \frac{1}{n} \ln C_e \tag{4}$$

where, Q_e and C_e are the same as in Langmuir isotherm, K_F and n are the Freundlich constants K_F is related to the binding energy of the adsorbent and n is the heterogeneity factor, which measure the deviation from linearity of the adsorption. The adsorption will be favourable if the value will be in the range of 1 to 10. The plot between ln Q_e *vs.* ln C_e gives a straight line with slope $1/n$ and intercepts ln K_F as representing in Fig. 7b. The values of Freundlich constants are given in Table I. Both the isotherm experiments were carried out at room temperature. Based on the higher values of correlation coefficients R^2, the adsorption

data are depicted better by the Freundlich isotherm model than by the Langmuir isotherm model.

Table I. Coefficient of adsorption isotherm model with malachite green over ECO

Langmuir adsorption isotherm	Freundlich adsorption isotherm
Q_o = 43.47 mg g^{-1}	K_F = 9.876 (mg/g) (L/mg)$^{1/n}$
K_L = 0.0377 L mg^{-1}	1/n = 0.5491
R^2 = 0.7083	R^2 = 0.961

The photocatalysis of dyes was monitored by noting the decrease in absorbance of the dyes in presence samples under visible light irradiation. It was observed that the relative absorption intensity decreases as the visible light illumination contact period increases, which imply that the MG and CV dyes decompose gradually and their concentration decreases, while the rate of decrease was greater for MG than compared to CV. Initially, the rate of reaction increases with increase pH till 7.5, then the rate declines with increase in the pH value. This change happens due to the surface charge of catalyst and the point of zero charge which vary with change in pH.

The rate constant for the photodegradation of each dye was calculated from the plot of the absorbance and irradiation time. The rate constant of the photodegradation was determined using the expression:

$$k = \frac{1}{t} \ln \frac{A_o}{A_t} \tag{5}$$

where k and t are rate constant and time. The photocatalyst ECO was found to be more efficient in mineralization of MG dye (56.3 % in 100 min) in Table II and Fig.8a with higher reaction rate constant, when compared to CV (Table II and Fig. 8b). Also, the significant degradation of MG to 56.3 % was achieved in shorter time interval of less than 100 min of irradiation, whereas it took 190 min for CV to degrade 37.9 % (Table II). The degradation rate values were higher for both the dyes when compared with CO sample and also no self-decomposition of the dyes took place in absence of catalyst under the above similar conditions. Table III represent comparison with previous literature.

Under same photocatalyst, MG degradation was higher than CV, which exhibited that photocatalytic activity depends on the distinctive chemical structures of the dyes.

As reported by Ju *et al.* the degradation mechanism of CV and MG dye in aqueous solution followed a five step path: cleavage of central carbon atom, consequent decomposition of the p-π conjugated structure, *N*-demethylation reactions, adduct reactions, loss of benzene rings and ring opening reactions.[39,40] The probable mechanism is suggested in Scheme 1. CV first gets degraded into MG which further breaks down. Both dyes have para quinoid ring chromophores and

phenyl rings substituted at para position by positively charged *N*,*N*′-dimethyl amino auxochromes.

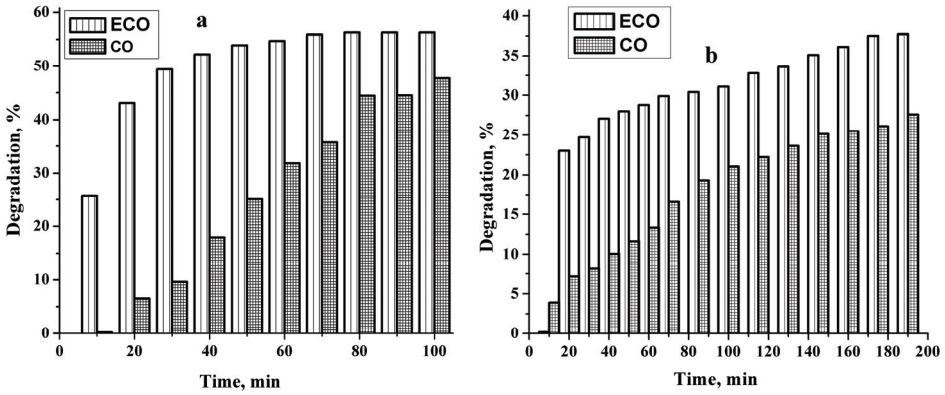

Fig. 8. Percentage degradation of: a) MG and b) CV dye in the presence ECO and CO.

TABLE II. Rate constants and degradation of dyes

Sample	MG Dye		CV dye	
	Rate constant, min^{-1}	Degradation, %	Rate constant, min^{-1}	Degradation, %
ECO	2.15×10^{-2}	56.3	4.0763×10^{-3}	37.9
CO	5.89×10^{-3}	47.7	2.9017×10^{-3}	27.6

TABLE III. Comparison of degradation of dyes

Co_3O_4 nanocatalyst, catalyst loading	Methodology	Pollutant dye	Time min	Degradation %
CoAc, urea and PEG, 0.5 g L^{-1} [36]	Hydrothermal	Methyl violet	120	50
Cobalt chloride, EG, PVP and hydrazine, 20 mg L^{-1} [29]	Hydrothermal	Methyl orange	100	70
Cobalt chloride, EG and sodium acetate, 10 mg L^{-1} [37]	Hydrothermal	Methyl orange	120	55
Cobalt nitrate, 1 g L^{-1} [38]	Sol–gel	Methylene blue	120	10

MG has two substituted rings while CV has three substituted rings which affect their spatial configuration. The two substituted rings in MG are coplanar whereas in CV the three rings are twisted out of the plane of the central conjugated ring which makes it more stable[41] suggesting that a large energy barrier is to be crossed to degrade CV into MG. EDTA, being a hexadentate ligand and effective capping agent has also been confirmed earlier with ZnO.[41] It is therefore critical to the formation of a protective layer as it gets chemisorbed as carboxylate onto the surface of cobalt oxide nanoparticles, altering their surface properties, which not only stabilizes them against agglomeration and aggregation but also prevents their aerial oxidation. As reported in literature the EDTA molecules

cap and confine the particle size to a great extent.[42] Porous structures on the surface allow greater adsorption of dye molecules and shorter diffusion path length of photogenerated charge carriers.[12] All the above factors contributed to the better performance of ECO for photocatalytically degradation the MG dye.

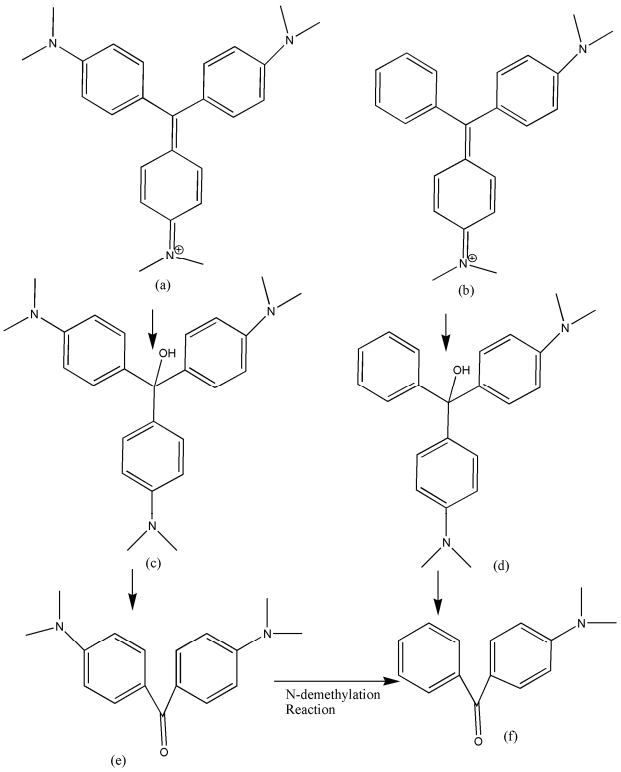

Scheme 1. Probable degradation mechanism of MG and CV dye (a – MG; b – CV; c and d – carbinol base; e – bis(4-(dimethylamino)phenyl)methanone; f – 4-dimethylaminobenzophenone).[39]

CONCLUSION

ECO and CO were synthesized by a sol–gel route and utilized as catalysts for the photocatalytic degradation of MG and CV dyes to reduce their toxicity. The nanomaterial revealed crystalline morphologies and good optical properties.

The ECO nanomaterial is found superior than CO and exhibited higher capacity for removal of MG and CV dyes from aqueous solution under visible light irradiations. This is due to the distinctive morphology, high surface area and high crystalline of synthesized EDTA supported Co_3O_4. The different rate of degradation of dyes was based on the specific stero-configuration of MG and CV dyes. Therefore, it could be concluded that ECO is one of the excellent active catalyst

for the removal of cationic basic dyes from water, especially MG. Photocatalytically degradation of dyes follow pseudo first order kinetics and are presented by the Freundlich adsorption isotherm.

Acknowledgements. The authors thank IIT Delhi and DST-SAIF, Kochi for sample analysis. DV would also like to acknowledge the support provided under the DST-FIST Grant No.SR/FST/PS-I/2019/68 of Govt. of India.

ИЗВОД

УЛОГА НАНОМАТЕРИЈАЛА КОБАЛТ-ОКСИДА КАПТИРАНОГ СА EDTA У ФОТОКАТАЛИТИЧКОЈ РАЗГРАДЊИ БОЈА

MEENA SINGH[1], DIPTI VAYA[2], RAVI KUMAR[3] и BIJOY K. DAS[1]

[1]*Department of Applied Science, The NorthCap University, Sector 23A, Gurugram-122017, India,* [2]*Department of Chemistry, Amity School of Applied Sciences, Amity University Haryana, Gurugram-122413, India и* [3]*Department of Chemistry, NIT, Srinagar, Jammu and Kasmir-190006, India*

Боје из текстила, фарби и других индустријских производа загађују одпадне воде. Функционални наноматеријали обезбеђују начин да се отпадне воде ефикасно и брзо пречисте, захваљујући томе што имају велику површину у односу на запремину. Испитивана је синтеза кобалт оксида каптираног са етилендиаминтетрасирћетном киселином (EDTA) и његова примена на уклањање малахитне зелене (MG) и кристално љубичасте (CV) боје. Карактеризација синтетисаног наноматеријала испитана је SEM, TEM, XRD, TGA, FT-IR и UV–Vis техникама. Наведени наноматеријал показује бољу фотокаталитичку деградацију боја од самог кобалт оксида. Кинетика деградације је псеудо-првог реда и одговара Фројндлиховој апсорпционој изотерми. Фотодеградација две наведене боје се објашњава морфологијом наноматеријала који омогућава ефикасну електрон/ /шупљина сепарацију.

(Примљено 11 јула, ревидирано 4. октобра, прихваћено 16. новембра 2020)

REFERENCES

1. J. H. Huang, K. L. Huang, S. Q. Liu, A. T. Wang, C. Yan, *Colloids Surfaces, A* **330** (2008) 55 (https://doi.org/10.1016/j.colsurfa.2008.07.050)
2. R. Kabbout, S. Taha, *Phys. Proc.* **55** (2014) 437 (https://doi.org/10.1016/j.phpro.2014.07.063)
3. M. B. Kasiri, N. Modirshahla, H. Mansouri, *Int. J. Ind. Chem.* **4** (2013) 3 (https://doi.org/10.1186/2228-5547-4-3)
4. L. Saikia, D. Bhuyan, M. Saikia, B. Malakar, D. K. Dutta, P. Sengupta, *Appl. Catal., A* **490** (2015) 42 (https://doi.org/10.1016/j.apcata.2014.10.053)
5. M. R. Hoffmann, S. T. Martin, W. Choi, D. W. Bahnemannt, *Chem. Rev.* **95** (1995) 69 (https://doi.org/10.1021/cr00033a004)
6. C. Hariharan, *Appl. Catal., A* **304** (2006) 55 (https://doi.org/10.1016/j.apcata.2006.02.020)
7. E. A. Meulenkamp, *J. Phys. Chem., B* **102** (1998) 5566 (https://doi.org/10.1021/jp980730h)
8. K. S. Babu, A. R. Reddy, K. V. Reddy, *Mater. Res. Bull.* **49** (2014) 537 (https://doi.org/10.1016/j.materresbull.2013.09.024)
9. K. Sinkó, G. Szabó, M. Zrínyi, *J. Nanosci. Nanotechnol.* **11** (2011) 4127 (https://doi.org/10.1166/jnn.2011.3875)

10. S. Farhadi, J. Safabakhsh, P. Zaringhadam, *J. Nanostruct. Chem.* **3** (2013) 69 (https://doi.org/10.1186/2193-8865-3-69)
11. R. K. Gupta, A. K. Sinha, B. N. Raja Sekhar, A. K. Srivastava, G. Singh, S. K. Deb, *Appl. Phys., A* **103** (2011) 13(https://doi.org/10.1007/s00339-011-6311-6)
12. R. Edla, N. Patela, M. Orlandi, N. Bazzanella, V. Bello, C. Maurizio, G. Mattei, P. Mazzoldi, A. Miotello, *Appl. Catal., B* **166**–**167** (2015) 475 (https://doi.org/10.1016/j.apcatb.2014.11.060)
13. W. Wen, J. M. Wu, J. P. Tu, *J. Alloys Compd.* **513** (2012) 592 (https://doi.org/10.1016/j.jallcom.2011.11.019)
14. S. Baruah, J. Dutta, *Sci. Technol. Adv. Mater.* **10** (2009) 013001 (https://doi.org/10.1088/1468-6996/10/1/013001)
15. H. N. Azlina, J. N. Hasnidawani, H. Norita, S. N. Surip, *Acta Phys. Pol., A* **129** (2016) 842 (https://doi.org/10.12693/APhysPolA.129.842)
16. E. G. Goh, X. Xu, P. G. McCormick, *Scr. Mater.* **78**–**79** (2014) 49 (https://doi.org/10.1016/j.scriptamat.2014.01.033)
17. P. Chandrasekaran, G. Viruthagiri, N. Srinivasan, *J. Alloys Compd.* **540** (2012) 89 (https://doi.org/10.1016/j.jallcom.2012.06.032)
18. K. P. Singh, S. Gupta, A. K. Singh, S. Sinha, *J. Hazard. Mater.* **186** (2011) 1462 (https://doi.org/10.1016/j.jhazmat.2010.12.032)
19. W. Cheng, S. Wang, L. Lu, W. Gong, X. Liu, B. Gao, H. Zhang, *Biochem. Eng. J.* **39** (2008) 538 (https://doi.org/10.1016/j.bej.2007.10.016)
20. O. J. Hao, H. Kim, P. C. Chiang, *Crit. Rev. Environ. Sci. Technol.* **30** (2000) 449 (https://doi.org/10.1080/10643380091184237)
21. S. Li, *Bioresour. Technol.* **101** (2010) 2197 (https://doi.org/10.1016/j.biortech.2009.11.044)
22. K. V. K. Rao, *Toxicol. Lett.* **81** (1995) 107 (https://doi.org/10.1016/0378-4274(95)03413-7)
23. M. Saquib, M. Muneer, *Dyes Pigments* **56** (2003) 37.(https://doi.org/10.1016/S0143-7208(02)00024-4)
24. S. Ameen, M. S. Akhtar, M. Nazim, H. S. Shin, *Mater. Lett.* **96** (2013) 228 (https://doi.org/10.1016/j.matlet.2013.01.034)
25. L. Wang, B. Liu, S. Ran, H. Huang, X. Wang, B. Liang, D. Chen, G. Shen, *J. Mater. Chem.* **22** (2012) 23541 (https://doi.org/10.1039/c2jm35617a)
26. L. Man, B. Niu, H. Xu, B. Cao, J. Wang, *Mater. Res. Bull.* **46** (2011) 1097 (https://doi.org/10.1016/j.materresbull.2011.02.045)
27. S. Vijayakumar, A. Kiruthika Ponnalagi, S. Nagamuthu, G. Muralidharan, *Electrochim. Acta* **106** (2013) 500 (https://doi.org/10.1016/j.electacta.2013.05.121)
28. S. Bazgir, S. Farhadi, *Int. J. Nanodimension* **8** (2017) 284 (http://www.ijnd.ir/article_656340.html)
29. X. Zhao, Z. Pang, M. Wu, X. Liu, H. Zhang, Y. Ma, Z. Sun, L. Zhang, X. Chen, *Mater. Res. Bull.* **48** (2013) 92 (https://doi.org/10.1016/j.materresbull.2012.10.001)
30. S. Farhadi, G. Nadri, M. Javanmard, *Int. J. Nanodimension* **7** (2016) 201 (http://www.ijnd.ir/article_649420.html)
31. T. Umamath, J. A. Selvi, S. A. Kanimozhi, S. Rajendran, A. J. Amalraj, *Ind. J. Chem. Technol.* **15** (2008) 560 (http://nopr.niscair.res.in/handle/123456789/2870)
32. R. Y. Hong, T. T. Pan, H. Z. Li, *J. Magn. Magn. Mater.* **303** (2006) 60 (https://doi.org/10.1016/j.jmmm.2005.10.230)
33. R. Hong, T. Pan, J. Qian, H. Li, *Chem. Eng. J.* **119** (2006) 71 (https://doi.org/10.1016/j.cej.2006.03.003)

34. J. C. Liu, J. H. Jean, C. C. Li, *J. Am. Ceram. Soc.* **89** (2006) 882 (https://doi.org/10.1111/j.1551-2916.2005.00858.x)
35. Z. Li, Y. Zhu, *Appl. Surf. Sci.* **211** (2003) 315 (https://doi.org/10.1016/S0169-4332(03)00259-9)
36. D. E. Zhang, L. Z. Ren, X. Y. Hao, B. Bin Pan, M. Y. Wang, J. J. Ma, F. Li, S. A. Li, Z. W. Tong, *Appl. Surf. Sci.* **355** (2015) 547 (https://doi.org/10.1016/j.apsusc.2015.04.018)
37. Y. Chen, L. Hu, M. Wang, Y. Min, Y. Zhang, *Colloids Surfaces, A* **336** (2009) 64 (https://doi.org/10.1016/j.colsurfa.2008.11.018)
38. M. Pudukudy, Z. Yaakob, *Chem. Pap.* **68** (2014) 1087 (https://doi.org/10.2478/s11696-014-0561-7)
39. Y. Ju, J. Fang, X. Liu, Z. Xu, X. Ren, C. Sun, S. Yang, Q. Ren, Y. Ding, K. Yu, L. Wang, Z. Wei, *J. Hazard. Mater.* **185** (2011) 1489 (https://doi.org/10.1016/j.jhazmat.2010.10.074)
40. Y. Ju, S. Yang, Y. Ding, C. Sun, A. Zhang, L. Wang, *J. Phys. Chem., A* **112** (2008) 11172 (https://doi.org/10.1021/jp804439z)
41. S. Meena, D. Vaya, B. K. Das, *Bull. Mater. Sci.* **39** (2016) 1735 (https://doi.org/10.1007/s12034-016-1318-4)
42. B. Ajitha, Y. A. Kumar Reddy, P. S. Reddy, H. J. Jeon, C. W. Ahn, *RSC Adv.* **6** (2016) 36171 (https://doi.org/10.1039/c6ra03766f).